

The novel Zn-doped hexagonal perovskite $\text{Ba}_7\text{In}_6\text{Al}_2\text{O}_{19}$: electrical conductivity and hydration

Irina Animitsa , Daniil Korona , Arina Bushueva,
Roman Andreev , Sergey Nokhrin

Institute of Natural Sciences, Ural Federal University, Ekaterinburg 620009, Russia

* Corresponding author: irina.animitsa@urfu.ru



This paper belongs to a Regular Issue.

Abstract

The novel phase $\text{Ba}_7\text{In}_{5.9}\text{Zn}_{0.1}\text{Al}_2\text{O}_{18.95}$ with hexagonal perovskite structure was obtained by solid-state technique. The substitution of In^{3+} by the Zn^{2+} leads to the expansion of the lattice parameters and cell volume. It was established that the investigated sample is capable of water incorporation from the gas phase; the degree of hydration reaches 1.42 mol H_2O , which is significantly higher than that for the undoped phase (0.41 mol H_2O). This is a result of the expansion of the hexagonal layer that facilitates the placement of OH^- -groups. The oxide-ion and proton conductivities for the doped $\text{Ba}_7\text{In}_{5.9}\text{Zn}_{0.1}\text{Al}_2\text{O}_{18.95}$ sample were higher than those for the undoped composition, $\text{Ba}_7\text{In}_6\text{Al}_2\text{O}_{19}$, by 0.50 and 0.75 orders of magnitude (500 °C), respectively. The new phase $\text{Ba}_7\text{In}_{5.9}\text{Zn}_{0.1}\text{Al}_2\text{O}_{18.95}$ demonstrates the predominant protonic conductivity at $T \leq 500$ °C and $p\text{H}_2\text{O} = 1.93 \cdot 10^{-2}$ atm.

Keywords

hexagonal perovskite
proton conductivity
hydration
transport numbers

Received: 24.08.24
Revised: 09.09.24
Accepted: 11.09.24
Available online: 30.09.24

Key findings

- A novel hexagonal perovskite $\text{Ba}_7\text{In}_{5.9}\text{Zn}_{0.1}\text{Al}_2\text{O}_{18.95}$ has been synthesized.
- $\text{Ba}_7\text{In}_{5.9}\text{Zn}_{0.1}\text{Al}_2\text{O}_{18.95}$ is capable of dissociative water molecule incorporation.
- $\text{Ba}_7\text{In}_{5.9}\text{Zn}_{0.1}\text{Al}_2\text{O}_{18.95}$ is able to exhibit proton conductivity.
- $\text{Ba}_7\text{In}_{5.9}\text{Zn}_{0.1}\text{Al}_2\text{O}_{18.95}$ demonstrates predominant proton transport at $T \leq 500$ °C in wet air.
- The Zn^{2+} -doping of $\text{Ba}_7\text{In}_6\text{Al}_2\text{O}_{19}$ increases the oxide-ion and proton conductivities.

© 2024, the Authors. This article is published in open access under the terms and conditions of the Creative Commons Attribution (CC BY) license (<http://creativecommons.org/licenses/by/4.0/>).

1. Introduction

High-temperature proton conductors, first described by H. Iwahara more than 40 years ago [1, 2], are still being intensively studied, since they are promising electrolytes for solid oxide fuel cells, which are highly efficient, environmentally friendly and economically attractive electrochemical devices. At present, high values of proton conductivity have been achieved for acceptor-doped perovskites – barium cerates and zirconates $\text{Ba}(\text{Ce},\text{Zr})\text{O}_3$ [3–5], but their chemical stability is unsatisfactory due to degradation in atmospheres containing CO_2 [6–16]. Primarily, the creation of new proton-conducting complex oxides occurs both by modifying the composition of known compounds and by complicating the structure [17–19].

In the 20s, high-temperature proton transport was also discovered in a more complex structural type – hexagonal

perovskite-like compounds built according to the block principle from fragments of various structural types [20–23]. For example, the compounds $\text{Ba}_5\text{M}_2\text{Al}_2\text{ZrO}_{13}$ ($\text{M} = \text{Gd}, \text{Lu}, \text{Y}, \text{Sc}, \text{In}$) [24] and $\text{Ba}_5\text{M}_2\text{Al}_2\text{SnO}_{13}$ ($\text{Gd}, \text{Dy}, \text{Ho}, \text{Y}, \text{Tm}, \text{Yb}$) [25] can be represented as an intergrowth of a perovskite block $\text{Ba}(\text{Zr},\text{Sn})\text{O}_3$ and two oxygen-deficient blocks $\text{Ba}_2\text{M}^{3+}\text{AlO}_5$. Among them, the most conductive are the Er-containing phases $\text{Ba}_5\text{Er}_2\text{Al}_2\text{ZrO}_{13}$ and $\text{Ba}_5\text{Er}_2\text{Al}_2\text{SnO}_{13}$, although the relationship between the nature of the cations and the magnitude of proton conductivity is not yet clear. Owing to the presence of blocks containing unoccupied oxygen positions, such phases are capable of incorporating water without doping. For example, zirconates can incorporate 0.23 mol H_2O for $\text{Ba}_5\text{Er}_2\text{Al}_2\text{ZrO}_{13}$ and 0.30 mol H_2O for $\text{Ba}_5\text{In}_2\text{Al}_2\text{ZrO}_{13}$ [26]. Stannates $\text{Ba}_5\text{M}_2\text{Al}_2\text{SnO}_{13}$ ($\text{Gd}, \text{Dy}, \text{Ho}, \text{Y}, \text{Tm}, \text{and Yb}$) exhibited water uptakes within $0.48 \leq x \leq 1.00$ at 100 °C depending on the nature of the

rare earth metals [25]. Among these oxides, the phase that exhibited the greatest water uptake of 1 mol H₂O was Ba₅Er₂Al₂SnO₁₃ [25]. It is not yet possible to establish any specific relationships between nature of the elements in the compound and water uptake, as the experimental data are still very limited. However, since it has been clearly shown that the incorporation of water molecules occurs in the oxygen-deficient layer, its size will be an important characteristic of hydration.

Investigations of the influence of doping on transport properties have been performed only for Ba₅In₂Al₂ZrO₁₃ [26–29], and it has been shown that not only acceptor doping but also isovalent substitution can improve the ionic (O²⁻, H⁺) conductivity. That is, the role of the geometric factor in ion transport is obvious.

The other composition with a hexagonal perovskite structure Ba₇Nb₄MoO₂₀ is formed by a combination of perovskite and palmierite-like layers [19]. The compound is composed of isolated tetrahedral units that have a particular topology that allows water incorporation and fast ionic transport. The phase can incorporate 0.80 mol H₂O, and this value is close to the theoretical solubility limit of one water molecule per formula unit, corresponding to one oxygen vacancy per formula unit of Ba₇Nb₄MoO₂₀. A strategy to increase the oxide-ion conductivity of this phase involves the introduction of an element with a higher oxidation state (donor doping), such as molybdenum or tungsten, into the niobium positions. The positive effect is explained by filling interstitial oxygen sites. However, the effect of such substitution on proton transport is ambiguous. For example, proton conduction in Ba₇Nb₄MoO₂₀ is critically reduced when niobium is replaced by tungsten (+6) or chromium (+6) [30, 31].

A more complex example of intergrowth structure is Ba₇M³⁺₆Al₂O₁₉, in which the same oxygen-deficient blocks Ba₂M³⁺AlO₅ (as for Ba₅M₂Al₂ZrO₁₃ [32]) are intergrown with a perovskite-like block Ba₃M³⁺₄O₉ ≡ Ba₃□M³⁺₄O₉□₃, containing barium and oxygen vacancies (□). The structures of all these compounds contain tetrahedra connected by their vertices and forming [Al₂O₇]-dimers, which alternate with octahedrally coordinated M³⁺-cations [33]. For such structures, the process of incorporating OH-groups is realized without acceptor doping and is due to the presence of coordination-unsaturated Ba²⁺-containing polyhedra in the hexagonal *h'*-layers. The degree of hydration is determined by the size of the interlayer space, which is sufficient to place the OH⁻-groups. Proton transport depends largely on the nature of the cation located in the octahedron and on the degree of ordering of the cations in the tetrahedra and octahedra.

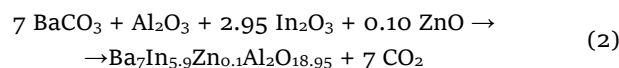
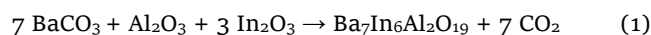
Summarizing the scientific literature on proton transport in hexagonal perovskites, we can conclude that there is no general strategy for optimizing proton transport in such structures yet. The state of the issue is still at the stage of accumulation of the experimental material. In

structural terms, such compounds are significantly more complex than classical perovskites ABO₃; therefore, establishing the «structure-defect structure-properties» correlation is a very difficult task.

We recently reported proton and oxide-ion conduction in the cation- and oxygen-deficient hexagonal perovskite Ba₇In₆Al₂O₁₉ [34]. However, acceptor doping has not been previously performed for this phase, and its effect on hydration and transport properties has not been studied. In this work, we prepared a new complex oxide in which some of the indium ions are replaced by zinc Ba₇In_{5.9}Zn_{0.1}Al₂O_{18.95}. We showed that with increasing lattice parameters and increasing number of oxygen vacancies the degree of hydration increased, and proton and oxide ion transport improved. Doping significantly increased the ionic transport numbers.

2. Experimental

The Zn²⁺-doped phase Ba₇In_{5.9}Zn_{0.1}Al₂O_{18.95} and the parent compound Ba₇In₆Al₂O₁₉ were prepared by a solid state technique according to the following reactions:



The preliminary dried starting reagents BaCO₃ (99.9999% purity, REACHIM, Russia), In₂O₃ (99.99% purity, REACHIM, Russia), Al₂O₃ (99.99% purity, REACHIM, Russia), ZnO (99.99% purity, REACHIM, Russia) were weighed in stoichiometric quantities, then ground in an agate mortar with ethanol. The calcination of the powder mixtures was performed according to the following scheme: 800, 1000, 1100 °C (24 h at each stage), with intermediate grinding after each heating step. The ceramic samples were obtained by pressing powders in cylindrical pellet form and sintering at 1250 °C for 24 h. The relative densities, measured from the mass and dimensions of the sintered pellets, were ~95% of the theoretical X-ray density.

The phase purity was studied via powder X-ray diffraction XRD on a Bruker Advance D8 diffractometer with Cu Kα radiation. The crystal structures of hydrated and dehydrated samples were checked by Rietveld refinement using FULLPROF software. For the XRD and TG investigations the dehydrated samples were prepared by heat treatment at 1100 °C for 3 h and then cooled in dry argon (pH₂O = 3.5·10⁻⁵ atm). The hydrated samples were obtained by slow cooling from 1100 to 150 °C (1 °C/min) under a flow of wet argon (99.999% purity, pH₂O = 1.93·10⁻² atm).

TG investigations were carried out on a Simultaneous Thermal Analyzer STA 409 PC analyzer (Netzsch) coupled with a quadrupole mass spectrometer QMS 403 C Aëolos (Netzsch). The samples were heated at the rate of

10 °C/min in the temperature range of 40–1100 °C under a flow of Ar in a corundum crucible. For TG measurements the powder samples were hydrated as described above.

For electrical measurements both opposite surfaces of the tablet were coated with Pd-Ag paste electrodes, and then the electrodes were fired at 1000 °C for 3 h. The AC conductivity of the samples was measured by the 2-probe method using a Z-1000P impedance spectrometer (Elins, RF) within the frequency range of 1–10⁶ Hz. The bulk resistances were calculated from the complex impedance plot using the Zview software fitting.

The conductivity measurements were performed at varying temperature under dry and wet air. The temperature dependencies were measured with a cooling rate of 10/min over the temperature range of 300–900 °C every 10–20 °C; at each temperature the sample was kept until the constant resistance values were attained. The «wet» atmosphere was obtained by bubbling the gas at room temperature first through distilled water and then through saturated solution of KBr ($p_{\text{H}_2\text{O}} = 1.93 \cdot 10^{-2}$ atm). The «dry» atmosphere was produced by circulating the gas through P₂O₅ ($p_{\text{H}_2\text{O}} = 3.5 \cdot 10^{-5}$ atm). The humidity of gases was monitored by an H₂O sensor («Honeywell» HIH-3610, USA).

The measurements of conductivities vs p_{O_2} were carried out in the temperature range of 500–800 °C by an electrochemical method using an electrochemical pump and an oxygen sensor (both based on yttrium-stabilized zirconium oxide), connected to the Zirconia-M automatic regulator [35]. The range of oxygen partial pressure was 10⁻¹⁸–0.21 atm. The measurements were performed under dry and wet atmospheres. The «wet» atmosphere was obtained by circulating the gas at room temperature through saturated solution of KBr ($p_{\text{H}_2\text{O}} = 1.93 \cdot 10^{-2}$ atm); the «dry» atmosphere was produced by circulating the gas through P₂O₅ ($p_{\text{H}_2\text{O}} = 3.5 \cdot 10^{-5}$ atm).

3. Results and Discussions

3.1. X-ray phase analysis

Room temperature X-ray diffraction (XRD) results showed that the sample Ba₇In_{5.9}Zn_{0.1}Al₂O_{18.95} was single phase and characterized by hexagonal symmetry (space group P6₃/mmc). Figures 1a and b present an example of profile fitting for the Ba₇In_{5.9}Zn_{0.1}Al₂O_{18.95} sample and the crystal structure, respectively. The obtained lattice parameters and cell volumes are shown in Table 1. The cell parameters for the undoped Ba₇In₆Al₂O₁₉ phase were in good agreement with the previously reported data [34]. The substitution of In³⁺ ions by Zn²⁺ leads to an increase in the unit cell parameters and the unit cell volume (Table 1) despite the smaller radius of the dopant ($r_{\text{In}^{3+}} = 0.80$ Å, $r_{\text{Zn}^{2+}} = 0.74$ Å for a coordination number of 6) [36]. We believe that this is due to the appearance of charged defects, which lead to additional repulsion between the layers. It should be said that similar effects were observed for doped phases with the Ruddlesden-Popper structure. For example, the introduction of a

dopant with a smaller ionic radius with respect to the host atoms causes lattice expansion, which was previously described for RP structures [37–39].

The incorporation of water was accompanied by an increase in the lattice parameters (more significant for the c parameters) and, accordingly, an increase in the cell volumes (Table 1). This behavior is typical for layered structures, which indicates the predominant location of the OH⁻ groups in the interlayer space, that is, in the oxygen-deficient *h'*-layer in our case (this corresponds to a more significant increase in the c parameter). Hydrolytic decomposition of the phases did not occur; no impurity phases were detected.

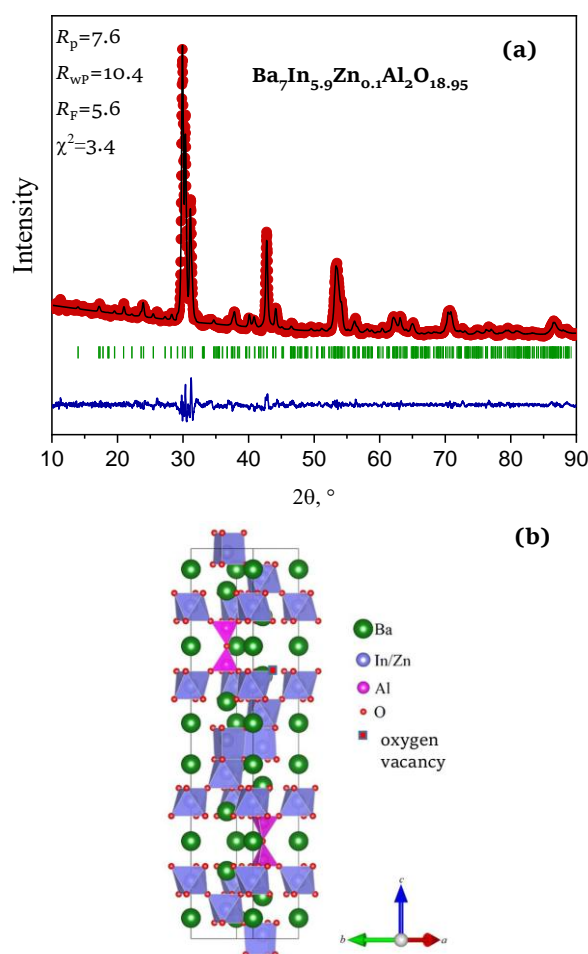


Figure 1 Rietveld profile fitting of powder X-ray diffraction pattern for the dehydrated Ba₇In_{5.9}Zn_{0.1}Al₂O_{18.95} sample. The experimental data are given as red circles, the fitted profile as solid black line. The vertical bars indicate the expected positions of the Bragg peaks upon refinement in the space group P6₃/mmc. The bottom blue line represents the difference between the calculated and experimental data (a). Crystal structures of the investigated sample (b).

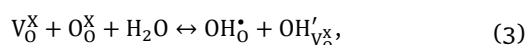
Table 1 Unit cell parameters and cell volumes for dehydrated Ba₇In₆Al₂O₁₉, Ba₇In_{5.9}Zn_{0.1}Al₂O_{18.95} samples and hydrated Ba₇In₆Al₂O₁₉ · 0.41H₂O, Ba₇In_{5.9}Zn_{0.1}Al₂O_{18.95} · 1.42H₂O samples.

Phase	a, Å	c, Å	V, Å ³
Ba ₇ In ₆ Al ₂ O ₁₉	5.921(2)	37.717(4)	1145.2(3)
Ba ₇ In _{5.9} Zn _{0.1} Al ₂ O _{18.95}	5.968(9)	38.055(4)	1174.1(8)
Ba ₇ In ₆ Al ₂ O ₁₉ · 0.41H ₂ O	5.925(7)	37.721(2)	1147.5(4)
Ba ₇ In _{5.9} Zn _{0.1} Al ₂ O _{18.95} · 1.42H ₂ O	5.970(3)	38.079(5)	1175.5(5)

3.2. Hydration processes

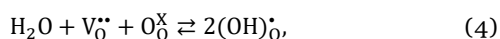
The possibility of water uptake can be established by TG measurements coupled with mass spectrometry (MS) analysis. Figure 2 shows TG and MS(H₂O)-curves for the preliminarily hydrated Ba₇In_{5.9}Zn_{0.1}Al₂O_{18.95} sample in comparison with the TG curve of the undoped phase. The main mass loss occurs in the temperature range of 150–500 °C, which is accompanied by two MS(H₂O) effects. In addition, at a high temperature ~750 °C there is also a slight loss of mass due to the release of water, which is the third effect on the MS(H₂O) curve. Mass stabilization occurs above 900 °C. Thus, the Zn²⁺-doped sample is capable of hydration, and the degree of hydration was 1.42 mol H₂O which is significantly greater than that of the undoped phase (0.41 mol H₂O).

The formation of proton defects for phases with unoccupied crystallographic oxygen positions can be described by the following quasi-chemical reactions in the Kröger-Vink notation:



where V_O^X is the structural oxygen vacancy, O_O^X is the oxygen atom in a regular position, OH_O^\bullet is the hydroxyl group in the oxygen sublattice, $OH_{V_O^X}'$ is the hydroxyl group in the position of the structural oxygen vacancy.

On the other hand, the oxygen vacancies that appear during acceptor doping $V_O^{\bullet\bullet}$ are also capable of incorporating protons (OH-groups):



where $V_O^{\bullet\bullet}$ – oxygen vacancy, OH_O^\bullet – hydroxyl group in the oxygen sublattice. These equations demonstrate the correlation between the concentration of oxygen vacancies and the degree of hydration (i.e., the concentration of protons).

However, the effect of increasing the degree of hydration is not due to additional oxygen deficiency as a result of doping, since it is more significant than the resulting concentration of oxygen vacancies. That is, the appearance of oxygen vacancies [$V_O^{\bullet\bullet}$] = 0.05 upon doping does not correspond to such significant increase in the concentration of protons (increase by 1 mole of water). As it is known, the ability of phases with a block (layered) structure to hydrate occurs without acceptor doping and is due to the introduction of OH⁻-groups into the interlayer space [23]. Accordingly, the solubility limit for such phases does not correlate with the concentration of oxygen vacancies, but is determined by the sufficient space to place OH⁻-groups. Thus, the solubility limit is determined by changing the geometric factor, that is, increasing the cell parameters in our case. As mentioned earlier [34], the capability of the compound Ba₇In₆Al₂O₁₉ to incorporate water is due to the presence of oxygen-deficient hexagonal layers, where barium is bonded in a 9-coordinate geometry (i.e. with nine oxygen atoms) [40]. Accordingly, such

coordinatively unsaturated barium polyhedron can incorporate OH⁻-groups and increase its coordination number. Thus, sufficient space in the hexagonal layers is necessary for the arrangement of OH⁻ groups. Consequently, an increase in the cell volume during doping facilitates an increase in water uptake. Therefore, the strategy of increasing the cell volume and, as a consequence, the size of the interlayer space is successful for increasing the proton concentration in compounds with hexagonal structures. Such features of the hydration character of block (layered) phases distinguish them from classical doped perovskites, for which a correlation between the concentration of oxygen vacancies and the concentration of protons is observed.

3.3. Electrical conductivity

3.3.1. Dry conditions

In Figure 3 the evolution of the impedance spectra of Ba₇In_{5.9}Zn_{0.1}Al₂O_{18.95} sample is shown as a Nyquist plot for several temperatures. This view of the spectra was typical of the investigated compounds under different experimental conditions. As can be seen, three semicircles in the complex $Z'-Z''$ plane, corresponding to the bulk, grain-boundary and electrode components were observed. The main contribution is represented by the grain boundary process; these semicircles have capacitances of ~10⁻¹⁰–10⁻⁹ F·cm⁻¹. The capacitance for the first semicircle, starting from the «O»-coordinates and representing the bulk response, is determined to be ~10⁻¹¹ F·cm⁻¹; the capacitance for the third low-frequency semicircle, representing the electrode response, is ~10⁻⁷–10⁻⁶ F·cm⁻¹.

The calculated bulk, grain-boundary and total conductivities of Ba₇In_{5.9}Zn_{0.1}Al₂O_{18.95} as a function of temperature are shown in Figure 4. The grain boundary conductivity is more than one order of magnitude lower than the bulk conductivity, and the total conductivity is determined by the grain boundary conductivity (for both dry and wet air).

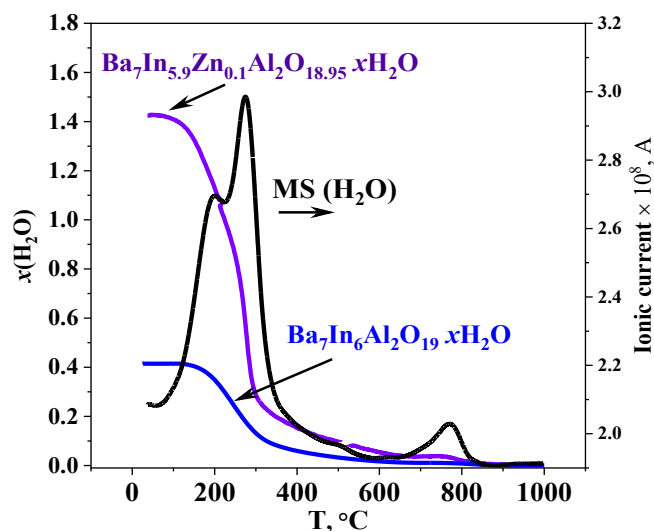


Figure 2 TG and MS(H₂O) curves for Ba₇In_{5.9}Zn_{0.1}Al₂O_{18.95}, and the TG curve for Ba₇In₆Al₂O₁₉.

There are little data in the literature concerning the analysis of hodographs for hexagonal perovskites and the extraction of different contributions, and most of the data show only conductivity dependences. However, a number of articles have shown that for such structures a more significant contribution of grain boundaries is observed [25, 41, 42]. The general explanation is that the state of the grain boundaries differs from the bulk, but an analysis of the reasons requires separate studies.

The electrode response observed in the low-frequency region is represented by a very small semicircle (that is, low polarization resistance), which indicates the reversibility of the electrodes.

A comparison of the conductivities of the doped and undoped samples is shown in Figure 5. The conductivity of the Zn²⁺-doped phase is higher than that of the pure phase over the entire studied temperature range, which is presumably due to the formation of oxide-ion vacancies as a result of the replacement of In³⁺ with Zn²⁺. The differences reached half an order of magnitude. To separate the total conductivity into partial contributions, the conductivity was measured vs the partial oxygen pressure.

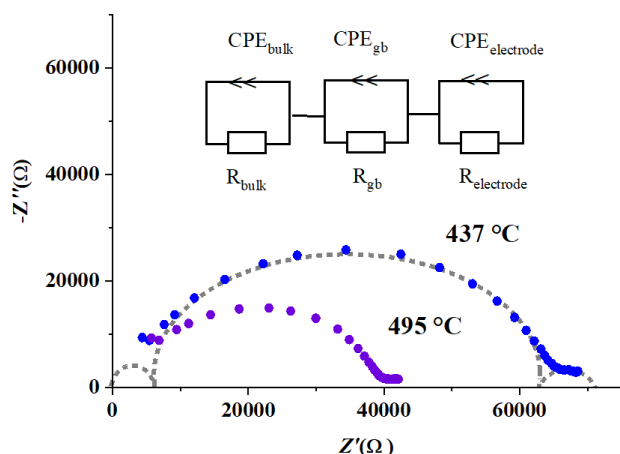


Figure 3 Impedance spectra of Ba₇In_{5.9}Zn_{0.1}Al₂O_{18.95} at different temperatures in dry air ($p_{\text{H}_2\text{O}} = 3.5 \cdot 10^{-5}$ atm).

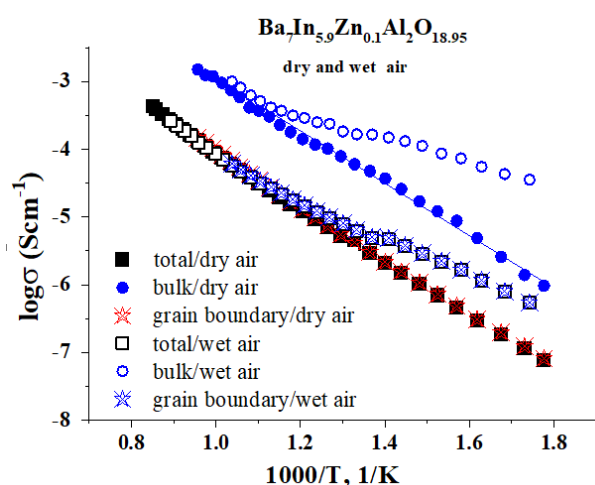
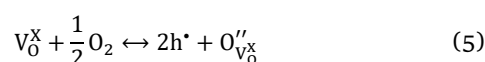


Figure 4 Temperature dependencies of the bulk, grain-boundary and total conductivities for Ba₇In_{5.9}Zn_{0.1}Al₂O_{18.95} in dry ($p_{\text{H}_2\text{O}} = 3.5 \cdot 10^{-5}$ atm, filled signs) and wet ($p_{\text{H}_2\text{O}} = 1.93 \cdot 10^{-2}$ atm, open signs) air.

Figure 6 shows a comparison of the dependencies of the conductivities vs the oxygen partial pressure at different temperatures for dry conditions ($p_{\text{H}_2\text{O}} = 3.5 \cdot 10^{-5}$ atm) for the samples Ba₇In_{5.9}Zn_{0.1}Al₂O_{18.95} and Ba₇In₆Al₂O₁₉. Both samples exhibited a plateau region in the range of oxygen partial pressures $10^{-18} \leq p_{\text{O}_2} \leq 10^4$ atm. The independence of conductivity from p_{O_2} indicates the dominant ionic nature of conductivity; taking into account the specificity of disordering, namely, the presence of oxygen deficiency, it can be concluded that the nature of ionic conductivity is oxide-ionic. As can be seen, the ionic conductivity of Zn²⁺-doped phase is higher than that of the parent phase.

Under oxidizing conditions ($p_{\text{O}_2} > 10^{-4}$ atm) the conductivity increased with increasing p_{O_2} , which indicates the appearance of a contribution of hole conductivity. The formation of holes can be described by the following quasi-chemical equation:



where V_0^X is the structural oxygen vacancy, O_{V_0}'' is the oxygen atom in the position of the structural oxygen vacancy, h^* is the hole.

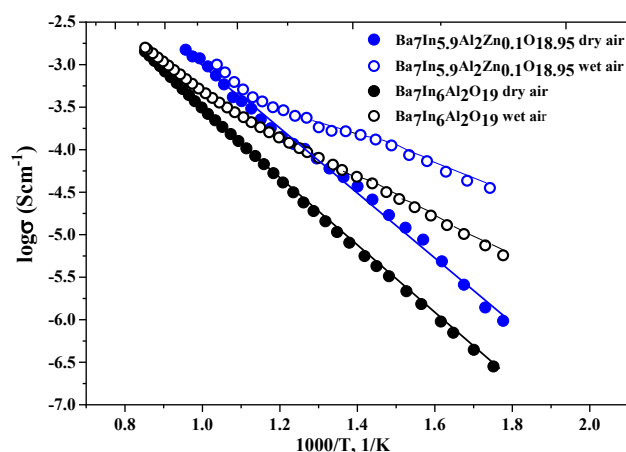


Figure 5 Comparison of the temperature dependencies of the conductivities of doped Ba₇In_{5.9}Zn_{0.1}Al₂O_{18.95} and undoped Ba₇In₆Al₂O₁₉ samples in dry ($p_{\text{H}_2\text{O}} = 3.5 \cdot 10^{-5}$ atm, filled signs) and wet ($p_{\text{H}_2\text{O}} = 1.93 \cdot 10^{-2}$ atm, open signs) air.

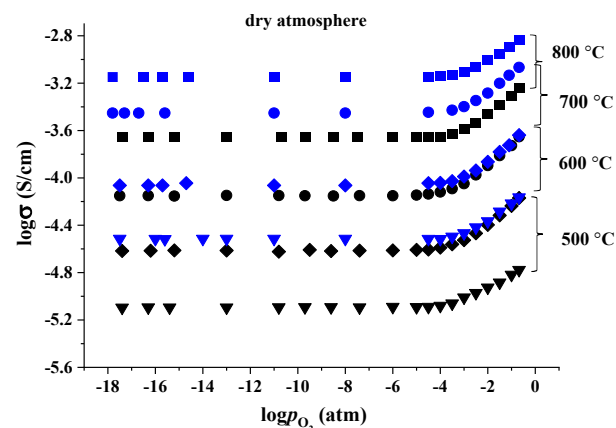


Figure 6 Dependencies of the conductivity vs oxygen partial pressure at different temperatures for Ba₇In_{5.9}Zn_{0.1}Al₂O_{18.95} (blue symbols) and Ba₇In₆Al₂O₁₉ (black symbols) in a dry atmosphere.

The ionic transport numbers, calculated as $t_{O^{2-}} = \sigma_{O^{2-}}/\sigma_{tot}$ ($\sigma_{O^{2-}}$ - conductivity in the plateau region, σ_{tot} - total conductivity in air $p_{O_2} = 0.21$ atm) are shown in Table 2. The $Ba_7In_{5.9}Zn_{0.1}Al_2O_{18.95}$ sample exhibited mixed conductivity in air, and the oxygen-ionic transport numbers increased slightly with increasing temperature.

The temperature dependences of the oxide-ion conductivity of the doped phase and the parent phase are shown in Figure 7. The oxide-ion conductivity of the doped phase is higher by approximately 0.5 orders of magnitude over the studied temperature range. This can be explained, on the one hand, by an increase in the disordering of the oxygen sublattice, and on the other hand, by an increase in the lattice parameters, since an increase in the lattice parameters leads to a decrease in the metal-oxygen bond energy and facilitates ion transport. The activation energy of the oxide-ion conductivity was 0.89 eV, which is typical of the oxygen transport, and this value was close to the activation energy of the undoped phase.

3.3.2. Wet conditions

As seen from the temperature dependences of the conductivities (Figure 5), an increase in humidity is accompanied by a significant increase in conductivity (up to 1.5 orders of magnitude at 300 °C) and a decrease in the activation energy. This indicates the appearance of a proton contribution to the conductivity. According to thermogravimetry measurements (Figure 2), the intense change in mass as a result of the intercalation of water molecules into the crystal lattice occurs at temperatures below 600 °C. So, the increase in conductivity in a wet atmosphere compared with dry air and the decrease in activation energy at temperatures below 600 °C are due to the contribution of proton conductivity. At higher temperatures, the conductivities in dry and wet atmospheres are almost identical, which, according to TG data, corresponds to a sharp decrease in the proton concentration; accordingly, the contribution of proton conductivity decreases. The magnitude of the proton conductivity and its activation energy are discussed below.

The conductivity in wet air is also 0.75 orders of magnitude greater than that of the parent phase at 300 °C.

Figures 8, 9 show the results of the conductivity measurements under wet conditions as a function of the oxygen partial pressure for the Zn^{2+} -doped sample in comparison with the dry conditions and in comparison with the undoped phase $Ba_7In_6Al_2O_{19}$, respectively. In the region of oxygen partial pressures $10^{-18} \leq p_{O_2} \leq 10^{-2}$ atm, a plateau of conductivity independence is observed. This indicates the dominant ionic conductivity. In the region of $p_{O_2} > 10^{-2}$ atm, the conductivity increases slightly with increasing p_{O_2} , as a result of the insignificant contribution of hole conductivity, and at a temperature of 500 °C the conductivity is practically independent of p_{O_2} in the entire studied range of partial oxygen pressures, which indicates dominant ionic transport.

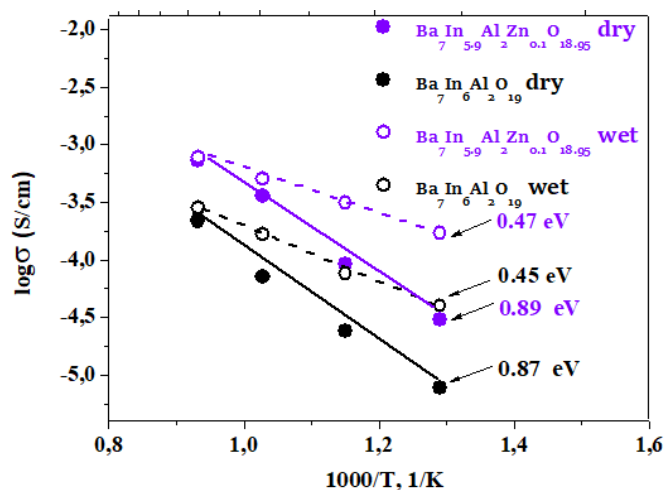


Figure 7 Temperature dependences of the ionic conductivities of $Ba_7In_{5.9}Zn_{0.1}Al_2O_{18.95}$ in comparison with $Ba_7In_6Al_2O_{19}$ for dry ($p_{H_2O} = 3.5 \cdot 10^{-5}$ atm, filled signs) and wet ($p_{H_2O} = 1.93 \cdot 10^{-2}$ atm, open signs) atmospheres.

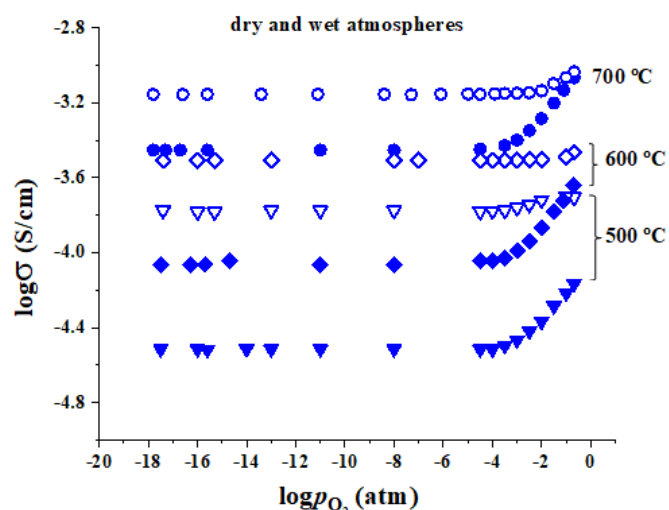


Figure 8 Dependencies of the conductivity vs oxygen partial pressure at different temperatures for $Ba_7In_{5.9}Zn_{0.1}Al_2O_{18.95}$ in dry (filled signs) and wet (open signs) atmospheres.

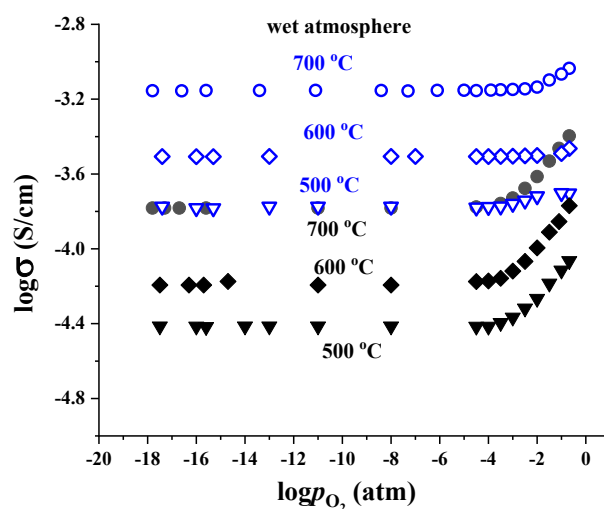


Figure 9 Dependencies of the conductivity vs oxygen partial pressure at different temperatures for $Ba_7In_{5.9}Zn_{0.1}Al_2O_{18.95}$ (blue signs) in comparison with $Ba_7In_6Al_2O_{19}$ (black signs) in a wet atmosphere.

A comparison of the conductivity isotherms of both the doped and undoped samples (Figure 9) revealed that the doped sample exhibited higher values of conductivity over the entire investigated pO_2 region.

The partial oxide-ion and proton conductivities were determined using data on conductivity as a function of oxygen partial pressure at different humidities. The calculations were made based on modeling in accordance with defect formation reactions, which were previously shown in the works [43–45].

In general, the conductivity in the plateau region is represented as a sum $\sigma = \sigma_{O^{2-}} + \sigma_{H^+}$. However, since the oxide-ion conductivity is significantly less than the proton conductivity, $\sigma_{O^{2-}} \ll \sigma_{H^+}$, at temperatures below 600 °C, the total conductivity is essentially the proton conductivity $\sigma \sim \sigma_{H^+}$. A comparison of the temperature dependences of the proton conductivities for the doped and parent phases is presented in Figure 7. In a wet atmosphere the conductivity of the doped phase is higher, and the difference reaches 0.75 orders of magnitude at 500 °C. That is, doping led to an increase in the proton conductivity. This is due to an increase in proton concentration according to the TG data. The proton conductivity is characterized by an activation energy of 0.47 eV, which is typical for proton conduction. The proton transport numbers calculated as $t_{H^+} = \sigma_{H^+}/\sigma_{tot}$ (air $pO_2 = 0.21$ atm, wet conditions) are presented in Table 2 confirm the abovementioned relationships.

Thus, the strategy of introducing zinc into the indium sublattice in hexagonal perovskite $Ba_7In_6Al_2O_{19}$ is promising in terms of both increasing the proton concentration and increasing the oxide-ion and proton conductivities.

A comparison of the temperature dependences of conductivity in wet air for the Zn^{2+} -doped sample $Ba_7In_{5.9}Zn_{0.1}Al_2O_{18.95}$ with other phases with a block (layered) structure is shown in Figure 10. The conductivity of the studied phase was lower than the conductivity of the best proton conductors with a hexagonal structure. However, at the same time, these conductivity values are typical of many phases and are within the limits of acceptable conductivity values for the proton-conducting electrolytes. Since for such structures variation in composition can significantly affect proton conductivity, it is obvious that to optimize the proton conductivity it is possible to search for other compositions based on $Ba_7In_6Al_2O_{19}$ or to use the co-doping method.

4. Limitations

One of the limitations is the interpretation of the data on the significant increase in lattice parameters upon doping. At present, the difficulties are due to the complexity of the structural analysis, since this is a very complex structure and it is difficult to assign coordinates to the dopant, which will be done in the future when wider dopant concentrations will have been studied.

Table 2 Oxide-ion transport numbers (dry air, $pH_2O = 3.5 \cdot 10^{-5}$ atm) and proton transport numbers (wet air, $pH_2O = 1.93 \cdot 10^{-2}$ atm) for $Ba_7In_{5.9}Zn_{0.1}Al_2O_{18.95}$ (%).

Temperature, °C	500	600	700	800
$t_{O^{2-}}$	38	39	40	46
t_{H^+}	97	91	78	–

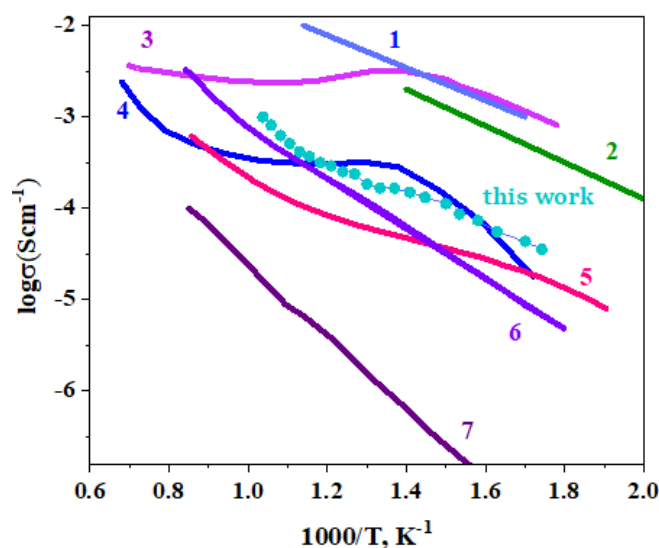


Figure 10 Comparison of the temperature dependences of the conductivities in wet air for $Ba_7Nb_{3.8}Mo_{1.2}O_{20.1}$ (1) [46], $Ba_7Nb_4MoO_{20}$ (2) [20], $Ba_5Er_2Al_2ZrO_{13}$ (3) [24], $Ba_5Lu_2Al_2ZrO_{13}$ (4) [24], $Ba_5In_2Al_2ZrO_{13}$ (5) [34], $BaLaIn_{0.5}Y_{0.5}O_4$ (6) [47], $BaLaInO_4$ (7) [47] and $Ba_7In_{5.9}Zn_{0.1}Al_2O_{18.95}$ (this work, circles).

5. Conclusions

In the present study the influence of the introduction of zinc into the indium sublattice of the hexagonal perovskite $Ba_7In_6Al_2O_{19}$ on hydration and conductivity was investigated.

The hexagonal perovskite $Ba_7In_{5.9}Zn_{0.1}Al_2O_{18.95}$ was synthesized by the solid-state method for the first time. The investigated phase had a hexagonal structure with a space group of $P6_3/mmc$. The substitution of In^{3+} by Zn^{2+} led to an increase in the lattice parameters. The lattice parameters for $Ba_7In_{5.9}Zn_{0.1}Al_2O_{18.95}$ were $a = 5.968(9)$ Å, $c = 38.055(4)$ Å vs $a = 5.921(2)$ Å, $c = 37.717(4)$ Å for $Ba_7In_6Al_2O_{19}$.

The studied sample $Ba_7In_{5.9}Zn_{0.1}Al_2O_{18.95}$ was capable of water incorporation and, in comparison with the undoped phase, a significant increase in the degree of hydration was observed (1.42 mol H_2O for $Ba_7In_{5.9}Zn_{0.1}Al_2O_{18.95}$ vs 0.41 mol H_2O for $Ba_7In_6Al_2O_{19}$). This is due to an increase in the cell volume and, as a consequence, an increase in the size of the oxygen-deficient hexagonal h'-blocks.

The electrical conductivity was investigated by the electrochemical impedance technique by varying T , pO_2 and pH_2O . It was found that Zn^{2+} doping led to an increase in oxygen-ion (dry conditions) and proton (wet conditions) conductivities due to increase in the concentration of oxygen vacancies and protons, respectively.

• Supplementary materials

No supplementary materials are available.

• Funding

This work was supported by the Russian Science Foundation and Government of the Sverdlovsk region (grant № 24-13-20026), <https://rscf.ru/project/24-13-20026/>.



• Acknowledgments

None.

• Author contributions

Conceptualization: I.E.A.

Methodology: I.E.A., D.V.K.

X-ray diffraction analysis: R.D.A.

TG measurements: D.V.K.

Conductivity measurements: A.V.B., S.S.N.

Writing – original draft: I.E.A.

Writing – review & editing: I.E.A., D.V.K.

• Conflict of interest

The authors declare no conflict of interest.

• Additional information

Author IDs:

Animitsa Irina, Scopus ID [6603520951](https://scopus.com/authid/detail.url?authorID=6603520951);

Daniil Korona, [13406057200](https://scopus.com/authid/detail.url?authorID=13406057200);

Arina Bushueva, [59307369500](https://scopus.com/authid/detail.url?authorID=59307369500);

Roman Andreev, [57737857400](https://scopus.com/authid/detail.url?authorID=57737857400);

Sergey Nokhrin, [56634307800](https://scopus.com/authid/detail.url?authorID=56634307800).

Website:

Ural Federal University, <https://urfu.ru/en/>.

References

- Takahashi T, Iwahara H. Solid state ionics: proton conduction in perovskite type solid solutions. *Rev Chim Miner.* 1980;17(4):243–253. doi:[10.1002/chin.198114014](https://doi.org/10.1002/chin.198114014)
- Iwahara H, Esaka T, Uchida H, Maeda N. Proton conduction in sintered oxides and its application to steam electrolysis for hydrogen production. *Solid State Ionics.* 1981;3–4:359–363. doi:[10.1016/0167-2738\(81\)90113-2](https://doi.org/10.1016/0167-2738(81)90113-2)
- Karuppiah K, Ashok A. Review on Proton and Oxide Ion Conducting Perovskite Materials for SOFC Applications. *Nanomater Energy.* 2019;8(1):1–8. doi:[10.1680/jnaen.18.00004](https://doi.org/10.1680/jnaen.18.00004)
- Medvedev D, Murashkina A, Pikalova E, Demin A, Podias A, Tsiakaras P. BaCeO₃: Materials development, properties and application. *Prog Mater Sci.* 2014;60:72–129. doi:[10.1016/j.pmatsci.2013.08.001](https://doi.org/10.1016/j.pmatsci.2013.08.001)
- Tayyab M, Rauf S, Khan AZ, Tayyab Z, Khan K, Hussain I, Hussain MB, Waseem M, Alodhayb AN, Fu XZ, Qasim M, Tian Y. Breaking barriers: Novel approaches to proton-conducting oxide materials. *Ceram Int.* 2024. doi:[10.1016/j.ceramint.2024.06.008](https://doi.org/10.1016/j.ceramint.2024.06.008)
- Scholten MJ, Schoonman J, van Miltenburg JC, Oonk HAJ. Synthesis of strontium and barium cerate and their reaction with carbon dioxide. *Solid State Ionics.* 1993;61:83–91. doi:[10.1016/0167-2738\(93\)90338-4](https://doi.org/10.1016/0167-2738(93)90338-4)
- Ma G, Shimura T, Iwahara H. Ionic conduction and non-stoichiometry in Ba_xCe_{0.90}Y_{0.10}O_{3-α}. *Solid State Ionics.* 1998;110:103–110. doi:[10.1016/S0167-2738\(98\)00130-1](https://doi.org/10.1016/S0167-2738(98)00130-1)
- Ryu KH, Haile SM. Chemical stability and proton conductivity of doped BaCeO₃-BaZrO₃ solid solutions. *Solid State Ionics.* 1999;125:355–367. doi:[10.1016/S0167-2738\(99\)00196-4](https://doi.org/10.1016/S0167-2738(99)00196-4)
- Radojkovic A, Zunic M, Savic SM, Brankovic G, Brankovic Z. Chemical stability and electrical properties of Nb doped BaCe_{0.9}Y_{0.1}O_{3-δ} as a high temperature proton conducting electrolyte for IT-SOFC. *Ceram Int.* 2013;39(1):307–313. doi:[10.1016/j.ceramint.2012.06.026](https://doi.org/10.1016/j.ceramint.2012.06.026)
- Kannan R, Singh K, Gill S, Furstenhaupt T, Thangadurai V. Chemically Stable Proton Conducting Doped BaCeO₃-No More Fear to SOFC Wastes. *Sci Rep.* 2013;3:1–5. doi:[10.1038/srep02138](https://doi.org/10.1038/srep02138)
- Medvedev DA, Lyagaeva JG, Gorbova EV, Demin AK, Tsiakaras P. Advanced materials for SOFC application: Strategies for the development of highly conductive and stable solid oxide proton electrolytes. *Prog Mater Sci.* 2016;75:38–79. doi:[10.1016/j.pmatsci.2015.08.001](https://doi.org/10.1016/j.pmatsci.2015.08.001)
- Medvedev D, Lyagaeva J, Plaksin S, Demin A, Tsiakaras P. Sulfur and carbon tolerance of BaCeO₃-BaZrO₃ proton-conducting materials. *J Power Sources.* 2015;273:716–723. doi:[10.1016/j.jpowsour.2014.09.116](https://doi.org/10.1016/j.jpowsour.2014.09.116)
- Sazinas R, Bernuy-Lopez C, Einarsrud M-A, Grande T. Effect of CO₂ exposure on the chemical stability and mechanical properties of BaZrO₃-ceramics. *J Am Ceram Soc.* 2016;99:3685–3695. doi:[10.1111/jace.14395](https://doi.org/10.1111/jace.14395)
- Lacz A, Silarska K, Piecha I, Pasierb P. Structure, chemical stability and electrical properties of BaCe_{0.9}Y_{0.1}O_{3-δ} proton conductors impregnated with Ba₃(PO₄)₂. *Int J Hydrog Energy.* 2016;41:13726–13735. doi:[10.1016/j.ijhydene.2016.06.009](https://doi.org/10.1016/j.ijhydene.2016.06.009)
- Somekawa T, Matsuzaki Y, Sugahara M, Tachikawa Y, Matsumoto H, Taniguchi S, Sasaki K. Physicochemical properties of Ba(Zr,Ce)O_{3-δ}-based proton-conducting electrolytes for solid oxide fuel cells in terms of chemical stability and electrochemical performance. *Int J Hydrog Energy.* 2017;42(26):16722–16730. doi:[10.1016/j.ijhydene.2017.04.26](https://doi.org/10.1016/j.ijhydene.2017.04.26)
- Stavarakakis E, West M, Johnston S, McIllwaine R, Poulidi D. Hydration, CO₂ stability and wireless electrochemical promotion studies on yttria-doped Ba(Ce,Zr)O₃ perovskites. *Ionics.* 2019;25:1243–1257. doi:[10.1007/s11581-019-02836-6](https://doi.org/10.1007/s11581-019-02836-6)
- Guo H, Li Y, Jiang L, Sha Y, Guoa S, Han D. Transport properties of the Ba(Zr,Ce,Y,Yb)O_{3-δ} proton conductor: the real role of co-substitution of Y and Yb. *J Mater Chem A.* 2024;12:5875–5884. doi:[10.1039/D3TA07486B](https://doi.org/10.1039/D3TA07486B)
- Saito K, Umeda K, Fujii K, Mori K, Yashima M. High Proton Conduction by Full Hydration in Highly Oxygen Deficient Perovskite. *J Mater Chem A.* 2024;12(22):13310–13319. doi:[10.1039/D4TA01978D](https://doi.org/10.1039/D4TA01978D)
- Yang X, Fernandez-Carrión AJ, Geng X, Kuang X. B-Site Deficient Hexagonal Perovskites: Structural Stability, Ionic Order-Disorder and Electrical Properties. *Prog Solid State Chem.* 2024;74:1–19. doi:[10.1016/j.progsolidstchem.2024.100459](https://doi.org/10.1016/j.progsolidstchem.2024.100459)
- Fop S, McCombie KS, Wildman EJ, Skakle JMS, Irvine JTS, Connor PA, et al. High oxide ion and proton conductivity in a disordered hexagonal perovskite. *Nat Mater.* 2020;19:752–775. doi:[10.1038/s41563-020-0629-4](https://doi.org/10.1038/s41563-020-0629-4)
- Fop S, McCombie KS, Wildman EJ, Skakle JMS, McLaughlin AC. Hexagonal perovskite derivatives: a new direction in the design of oxide ion conducting materials. *Chem Commun.* 2019;55:2127–2137. doi:[10.1039/C8CC09534E](https://doi.org/10.1039/C8CC09534E)
- Fop S. Solid oxide proton conductors beyond perovskites. *J Mater Chem A.* 2021;9:18836–18856. doi:[10.1039/d1ta03499e](https://doi.org/10.1039/d1ta03499e)
- Tarasova NA, Animitsa IE, Galisheva AO, Medvedev DA. Layered and Hexagonal Perovskites as Novel Classes of Proton-

- Conducting Solid Electrolytes. A Focus Review. *Electrochem Mater Technol.* 2022;1:20221004. doi:[10.15826/elmattech.2022.1.004](https://doi.org/10.15826/elmattech.2022.1.004)
24. Murakami T, Hester J, Yashima M. High Proton Conductivity in $\text{Ba}_5\text{Er}_2\text{Al}_2\text{ZrO}_{13}$, a Hexagonal Perovskite-Related Oxide with Intrinsically Oxygen-Deficient Layers. *J Am Chem Soc.* 2020;142:11653–11657. doi:[10.1021/jacs.0c02403](https://doi.org/10.1021/jacs.0c02403)
25. Matsuzaki K, Saito K, Ikeda Y, Nambu Y, Yashima M. High Proton Conduction in the Octahedral Layers of Fully Hydrated Hexagonal Perovskite-Related Oxides. *J Am Chem Soc.* 2024;146:18544–18555. doi:[10.1021/jacs.4c04325](https://doi.org/10.1021/jacs.4c04325)
26. Andreev R, Korona D, Anokhina I, Animitsa I. Proton and oxygen-ion conductivities of hexagonal perovskite $\text{Ba}_5\text{In}_2\text{Al}_2\text{ZrO}_{13}$. *Mater.* 2022;15(11):1–18. doi:[10.3390/ma15113944](https://doi.org/10.3390/ma15113944)
27. Andreev RD, Korona DV, Anokhina IA, Gilev AR, Animitsa IE. Transport properties of In^{3+} - and Y^{3+} -doped hexagonal perovskite $\text{Ba}_5\text{In}_2\text{Al}_2\text{ZrO}_{13}$. *Russ J Electrochem.* 2023;(59):190–203. doi:[10.1134/S1023193523030035](https://doi.org/10.1134/S1023193523030035)
28. Andreev RD, Animitsa IE Protonic transport in the novel complex oxide $\text{Ba}_5\text{Y}_{0.5}\text{In}_{1.5}\text{Al}_2\text{ZrO}_{13}$. *Ionics.* 2023;29(11):4647–4658. doi:[10.1007/s11581-023-05187-5](https://doi.org/10.1007/s11581-023-05187-5)
29. Andreev RD, Korona DV, Vlasov MI, Animitsa IE. Protonic ceramics $\text{Ba}_5\text{In}_{2-x}\text{Y}_x\text{Al}_2\text{ZrO}_{13}$ with the perovskite-related hexagonal structure for solid oxide fuel cells: synthesis, optical band gap and transport properties. *Ceram Int.* 2024. doi:[10.1016/j.ceramint.2024.04.227](https://doi.org/10.1016/j.ceramint.2024.04.227)
30. Suzuki Y, Murakami T, Fujii K, Hester JR, Yasui Y, Yashima M. Simultaneous reduction of proton conductivity and enhancement of oxide-ion conductivity by aliovalent doping in $\text{Ba}_7\text{Nb}_4\text{MoO}_{20}$. *Inorg Chem* 2022;61:7537–7545. doi:[10.1021/acs.inorgchem.2c00671](https://doi.org/10.1021/acs.inorgchem.2c00671)
31. Sakuda Y, Hester JR, Yashima M. Improved oxide-ion and lower proton conduction of hexagonal perovskite-related oxides based on $\text{Ba}_7\text{Nb}_4\text{MoO}_{20}$ by Cr^{6+} doping. *J Ceram Soc Jpn.* 2022;130:442–447. doi:[10.2109/jcersj2.21192](https://doi.org/10.2109/jcersj2.21192)
32. Shpanchenko RV, Abakumov AM, Antipov EV, Nistor, Tendeloo G, Amelinckx SJ. Structural study of the new complex oxides $\text{Ba}_{5-y}\text{Sr}_y\text{R}_{2-x}\text{Al}_2\text{Zr}_{1+x}\text{O}_{13+x/2}$ (R = Gd-Lu, Y, Sc). *Solid State Chem.* 1995;118:180–192. doi:[10.1006/jssc.1995.1329](https://doi.org/10.1006/jssc.1995.1329)
33. Shpanchenko RV, Nistor L, Tendeloo G, Amelinckx S, Antipov EV, Kovba LM. High-resolution electron microscopic study of $\text{Ba}_7\text{Sc}_6\text{Al}_2\text{O}_{19}$ and related phases. *J Solid State Chem.* 1994;113:193–204. doi:[10.1006/jssc.1994.1359](https://doi.org/10.1006/jssc.1994.1359)
34. Andreev R, Animitsa I. Transport properties of intergrowth structures $\text{Ba}_5\text{In}_2\text{Al}_2\text{ZrO}_{13}$ and $\text{Ba}_7\text{In}_6\text{Al}_2\text{O}_{19}$. *Appl Sci.* 2023;13(6):1–14. doi:[10.3390/app13063978](https://doi.org/10.3390/app13063978)
35. Zirconia Project. Available online: <https://zirconia-project.wordpress.com/devices/zirconiam/>
36. Shannon RD. Revised effective ionic radii and systematic studies of interatomic distances in halides and chalcogenides. *Acta Cryst.* 1976; A32:751–767. doi:[10.1107/S0567739476001551](https://doi.org/10.1107/S0567739476001551)
37. Tarasova N, Animitsa I, Galisheva A, Korona D. Incorporation and Conduction of Protons in Ca, Sr, Ba-Doped BaLaInO_4 with Ruddlesden-Popper Structure. *Mater.* 2019;12(10):1–14. doi:[10.3390/ma12101668](https://doi.org/10.3390/ma12101668)
38. Troncoso L, Alonso JA, Fernández-Díaz MT, Aguadero A. Introduction of interstitial oxygen atoms in the layered perovskite $\text{LaSrIn}_{1-x}\text{B}_x\text{O}_{4+6}$ system (B=Zr, Ti). *Solid State Ionics.* 2015;282:82–87. doi:[10.1016/j.ssi.2015.09.014](https://doi.org/10.1016/j.ssi.2015.09.014)
39. Aguadero A, Alonso JA, Martínez-Lope MJ, Fernández-Díaz MT, Escudero MJ, Daza L. In situ high temperature neutron powder diffraction study of oxygen-rich $\text{La}_2\text{NiO}_{4+\delta}$ in air: correlation with the electrical behaviour. *J Mater Chem.* 2006;16:3402–3408. doi:[10.1039/b605886h](https://doi.org/10.1039/b605886h)
40. Shpanchenko RV, Antipov EV, Paromova MV, Kovba LM. Crystal structure of $\text{Ba}_7\text{Sc}_6\text{Al}_2\text{O}_{19}$. *Zhurnal Neorganicheskoi Khimii.* 1991;136:1402–1407.
41. Unti LF Kultz, Grzebielucka EC, Chinelatto ASA, MatherGC, Chinelatto AL. Synthesis and electrical characterization of $\text{Ba}_5\text{Nb}_4\text{O}_{15}$ and $\text{Ba}_5\text{Nb}_{3.9}\text{M}_{0.1}\text{O}_{(15-\delta)}$ (M = Ti, Zr) hexagonal perovskites. *Ceram Int.* 2019;45:5087–5092. doi:[10.1016/j.ceramint.2018.11.211](https://doi.org/10.1016/j.ceramint.2018.11.211)
42. McCombie KS, Wildman EJ, Fop S, Smith RI, Skakle JMS, McLaughlin AC. The Crystal Structure and Electrical Properties of the Oxide Ion Conductor $\text{Ba}_3\text{WNB}_2\text{O}_{8.5}$. *J Mater Chem A.* 2018;6:5290–5295. doi:[10.1039/C7TA08989A](https://doi.org/10.1039/C7TA08989A)
43. Frade JR. Theoretical behavior of concentration cells based on ABO_3 perovskite materials with protonic and oxygen-ion conduction. *Solid State Ionics.* 1995;78:87–97. doi:[10.1016/0167-2738\(95\)00008-T](https://doi.org/10.1016/0167-2738(95)00008-T)
44. Baek HD. Modeling of electrical conductivity in high-temperature proton-conducting oxides. *Solid State Ionics.* 1998;110:255–262. doi:[10.1016/S0167-2738\(98\)00138-6](https://doi.org/10.1016/S0167-2738(98)00138-6)
45. Glöckner R, Neiman A, Larring Y, Norby T. Protons in $\text{Sr}_3(\text{Sr}_{1+x}\text{Nb}_{2-x})\text{O}_{9-3x/2}$ perovskite. *Solid State Ionics.* 1999;125:369–376. doi:[10.1016/S0167-2738\(99\)00197-6](https://doi.org/10.1016/S0167-2738(99)00197-6)
46. Sakuda Y, Murakami T, Avdeev M, Fujii K, Yasui Y, Hester JR, et al. Dimer-mediated cooperative mechanism of ultrafast-ion conduction in hexagonal perovskite-related oxides. *Chem Mater.* 2023;35:9774–9788. doi:[10.1021/acs.chemmater.3c02378](https://doi.org/10.1021/acs.chemmater.3c02378)
47. Tarasova N, Galisheva A, Animitsa I, Korona D, Davletbaev K. Novel proton-conducting layered perovskite based on BaLaInO_4 with two different cations in B-sublattice: Synthesis, hydration, ionic (O^{2-} , H^+) conductivity. *Int J Hydrog Energy.* 2022;47:18972–18982. doi:[10.1016/j.ijhydene.2022.04.112](https://doi.org/10.1016/j.ijhydene.2022.04.112)